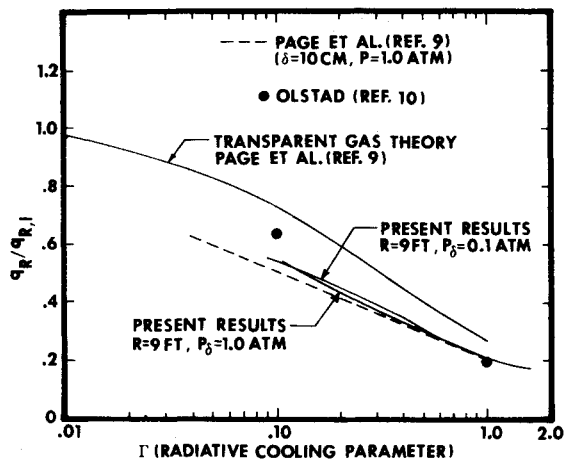

Fig. 3 Radiative heating vs radiative cooling parameter results.

value in the asymptote for δ/Δ appears to be approached. It is anticipated that for flight velocities higher than approximately 58,000 fps precursor radiation will become significant resulting in an increase in δ/Δ, since a portion of the energy lost by radiation through the shock wave which reduces the standoff distance will be absorbed by the oncoming gas and returned to the shock layer.

In the case of vertical entry (i.e., constant U_∞), the maximum collapse of the shock layer occurs along a line formed by conditions for $P_\delta \geqq 0.5$ atm. This contradicts Goulard's conclusion that the minimum δ/Δ would occur in the early part of atmospheric penetration.

In the case of near horizontal flight (i.e., constant P_δ) of a constant accelerating vehicle, radiationless shock layer thickness would occur followed by a linearly decreasing thickness. Further acceleration would result in a minimum and then increased thickness. This is in qualitative agreement with Goulard's conclusions.

The effects of radiation-gas dynamic coupling are also reflected in the radiative heating to the surface. Radiative heating rates from the present analysis are compared in nondimensional form with results of other investigators in Fig. 3. The present results correlate quite well with the radiative cooling parameter, Γ, and lie between the results of two inviscid shock layer analyses.[9,10] All of the shock layer results presented in Fig. 3 lie below the transparent gas theory results of Ref. 9. As pointed out by Page[9] the transparent theory is inadequate for predicting heating since the true optical properties of the shock layer are not uniformly optically thin. This result is certainly in accord with the results given in Fig. 2. The important point illustrated in Fig. 3 is that the radiative heating can be correlated with a single parameter, Γ, with little approximation and that both viscous and inviscid analyses yield similar results.

In conclusion, the radiation-gas dynamic coupling effect on the radiative heating can be related to the single parameter, Γ, whereas the effect on the shock layer thickness is not a simple function of this parameter.

References

[1] Goulard, R., "Preliminary Estimates of Radiative Transfer Effects on Detached Shock Layers," *AIAA Journal*, Vol. 2, No. 3, March 1964, pp. 494–502.

[2] Wilson, K. H., "Stagnation Point Analysis of Coupled Viscous-Radiating Flow with Massive Blowing," CR-1548, June 1970, NASA.

[3] Rigdon, W. S., Dirling, R. B., Jr., and Thomas, M., "Stagnation Point Heat Transfer During Hypervelocity Atmospheric Entry," CR-1462, Feb. 1970, NASA.

[4] Smith, G. L., Suttles, J. T., and Sullivan, E. M., "Viscous Radiating Flowfield on an Ablating Blunt Body," AIAA Paper 70-218, New York, 1970.

[5] Engel, C. D., Farmer, R. C., and Pike, R. W., "Ablation and Radiation Coupled Viscous Hypersonic Shock Layers," *AIAA Journal*, Vol. 11, No. 8, Aug. 1973, pp. 1174–1181.

[6] Hansen, C. F., "Approximations for Thermodynamic Properties of High Temperature Air," TR R-50, 1959, NASA.

[7] Inouye, M., "Blunt Body Solutions for Spheres and Ellipsoids in Equilibrium Gas Mixtures," TN D-2780, 1965, NASA.

[8] Hayes, W. D. and Probstein, R. F., *Hypersonic Flow Theory*, 2nd ed., Academic Press, New York, 1966.

[9] Page, W. A., Compton, D. L., Borucki, W. J., Ciffone, D. L., and Cooper, D. M., "Radiative Transport in Inviscid Nonadiabatic Stagnation-Region Shock Layers," *AIAA Progress in Astronautics and Aeronautics: Thermal Design Principles of Spacecraft and Entry Bodies*, Vol. 21, edited by Jerry T. Bevans, Academic Press, New York, 1969, pp. 75–114.

[10] Olstad, W. B., "Correlations for Stagnation-Point Radiative Heat Transfer," *AIAA Journal*, Vol. 7, No. 1, Jan. 1969, pp. 170–172.

Laminar Viscous-Inviscid Interactions at Transonic Speeds

DONALD J. COLLINS*
Jet Propulsion Laboratory, Pasadena, Calif.

Introduction

THE interaction between the boundary layer which forms on an aerodynamic surface and the inviscid outer flowfield is most pronounced at transonic speeds where the nature of the mixed supersonic and subsonic inviscid flowfield is often determined by the viscous portions of the flow. The early measurements by Ackeret et al.[1] and by Liepmann et al.[2] have explored some of the effects of viscosity and its influence on the over-all development of a transonic flowfield. More recently, the measurements reported by Alber et al.[3] have examined some of the details of a transonic turbulent boundary layer which separates either in the shock-interaction or in the pressure-gradient mode. In each of these investigations, it has been clear that a strong interaction exists between the viscous and the inviscid flows, and as a consequence the boundary layer cannot be treated theoretically as a small perturbation to the outer flow, but must be closely coupled with the outer flow, and must be solved simultaneously. The present Note will discuss some aspects of the laminar viscous-inviscid interaction at transonic speeds by examining data obtained on a 6% thick biconvex circular-arc airfoil and comparing the results with the predictions of Klineberg and Steger.[4]

Experimental Technique

The present experiments have been performed in the Jet Propulsion Lab. 20-in. wind tunnel at Mach numbers $0.6 \leqq M_\infty \leqq 0.915$ and Reynolds numbers $3.9 \times 10^4 \leqq Re \leqq 1.2 \times 10^6$, based on chord. Details of the model construction are given by Collins[5] and experimental details are given in Collins and Krupp.[6]

Received December 10, 1973; revision received February 28, 1974. This Note presents the results of one phase of research carried out at the Jet Propulsion Laboratory, under Contract NAS7-100, sponsored by NASA. The author would like to acknowledge the many valuable interactions with J. Krupp and J. Cole during the course of this research. Their contributions to this work have been both timely and numerous. Furthermore, the author wishes to acknowledge the excellent assistance of C. Nussey and R. Morrow and the entire Jet Propulsion Wind-Tunnel Staff in the performance of the experiments.

Index categories: Subsonic and Transonic Flow; Jets, Wakes, and Viscous-Inviscid Interactions.

* Senior Scientist, Physics Section. Member AIAA.

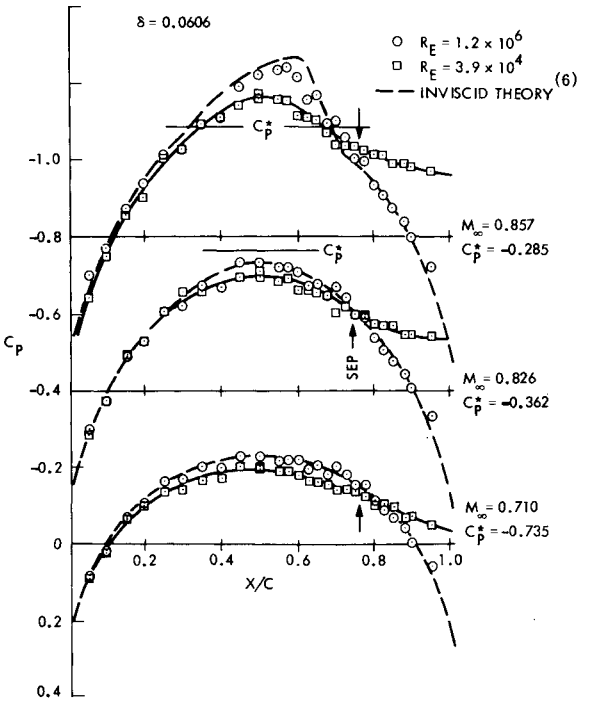

Fig. 1 Pressure distribution on the 6% biconvex airfoil comparing the effect of Reynolds number at various Mach numbers. Note offset scales.

Experimental Results

Laminar Pressure Distributions

The early data of Liepmann et al.[2] illustrated the major differences between laminar and turbulent shock wave-boundary layer interactions at transonic speeds. Further results which illustrate the influence of viscosity on the laminar separated transonic flowfield are presented in Fig. 1 where the pressure distributions obtained from a 6% thick biconvex airfoil at three Mach numbers are compared for Reynolds numbers 3.9×10^4, for which the flow is laminar, and 1.2×10^6 for which the flow on the airfoil is turbulent. The inviscid flow computations presented by Collins and Krupp[6] are included for comparison in each case. These results demonstrate that viscous effects are not localized at transonic speeds, and that the separation process results in a strongly interacting flowfield over the entire model. For the conditions represented in Fig. 1, little difference is seen near the leading edge between the data taken at $Re = 3.9 \times 10^4$ and at $Re = 1.2 \times 10^6$, for all Mach numbers. Downstream of the midchord, however, the effects of viscosity create substantial differences in the magnitude of the pressure coefficient. In each case, the laminar data shows a distinct separation point, with closure in the wake, whereas the turbulent data indicate no separation on the airfoil. At supercritical speeds, the transonic shock wave, evident in the turbulent data, degenerates to the gradual recompression evident in the laminar surface pressure distribution, although a clearly defined shock wave exists in the inviscid flow away from the model.

The pressure distributions obtained on the airfoil at low Reynolds numbers are shown in Figs. 2 and 3 as a function of the freestream Mach number. Figure 2 shows the results for a Reynolds number of 1.4×10^5, for which the boundary layer is laminar throughout the separation process. However, schlieren and shadowgraph photographs indicate that transition occurs near, and is probably responsible for, the location of the rear stagnation point in the wake. In each case, the pressure distribution upstream of separation, indicated by the arrow on each curve, agrees reasonably well with inviscid theory. Separation is observed to move upstream with increasing subcritical Mach number as a result of the increasing pressure gradient associated with the recompression over the rearward portion of the airfoil. When the flow becomes supercritical, a shock wave is formed, and the laminar boundary layer subsequently separates in the shock-interaction mode. As the Mach number is further increased, the shock wave and the separation point move downstream together.[7]

The pressure distributions shown in Fig. 3 were obtained at a Reynolds number of 3.9×10^4, for which the flow is completely laminar. For these data, Fig. 1 has shown that inviscid theory is no longer valid over the forward portion of the airfoil. This is a consequence both of the boundary-layer growth and of the extended recirculation zone which provides a significantly altered after-body and influences the fully coupled inviscid flowfield. The results in these two figures suggest that the over-all flowfield is dominated by a strong interaction between the viscous and the inviscid flowfields, and that attempts at the computation of these flows must include this strong coupling.

Comparison with Theory

Klineberg and Steger[4] have examined the transonic laminar flow over a circular-arc airfoil by using momentum integral techniques to compute the laminar boundary-layer development and an inviscid relaxation calculation to compute the outer flow. The inner and outer flows are computed iteratively, and are coupled at the outer edge of the boundary layer.

The results obtained from the present experiments are compared with the theory of Klineberg and Steger[4] in Fig. 4 for $Re = 1.4 \times 10^5$ and in Fig. 5 for $Re = 4 \times 10^4$. It is clear from these figures that the theoretical results overestimate the effects of viscosity and consequently predict values for the pressure coefficient which lie below the experimental data over the range of Mach numbers given. The effect becomes more pronounced with increasing Mach number. At $M_\infty = 0.910$, $Re = 1.4 \times 10^5$, for which the experiments in a solid-wall wind tunnel show the flow to be choked, the theory computed for an unbounded flow shows an isolated sonic bubble and a subsonic pressure plateau,

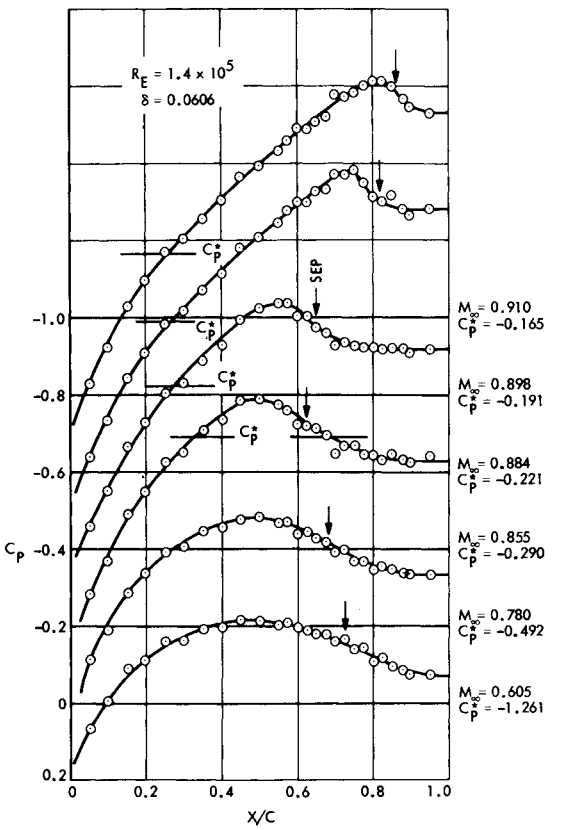

Fig. 2 Pressure distribution on the 6% biconvex airfoil as a function of Mach number for $Re = 1.4 \times 10^5$. Laminar boundary layer, transitional wake.

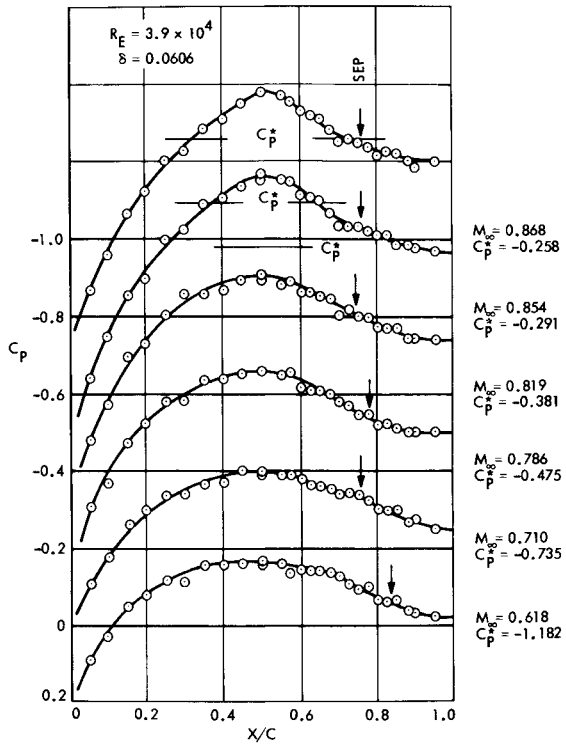

Fig. 3 Pressure distribution on the 6% biconvex airfoil as a function of Mach number for $Re = 3.9 \times 10^4$. Laminar boundary layer, laminar wake.

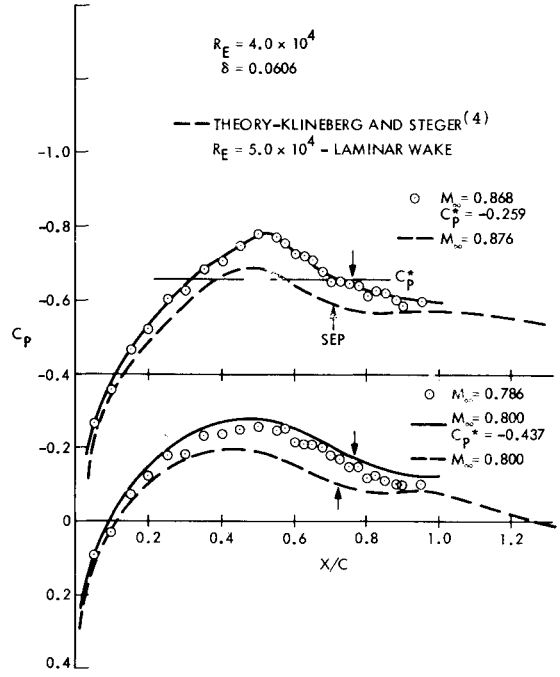

Fig. 5 Comparison of the pressure distribution on the 6% biconvex airfoil with the computations of Klineberg and Steger[4] for $Re = 4.0 \times 10^4$.

with separation occurring near sonic speed. Included in these laminar calculations is a calculation at $M_\infty = 0.808$ which includes the effect of a turbulent wake. This change has the effect of increasing the peak value of C_p, but the over-all agreement is not qualitatively changed on the airfoil. The location of separation is included on each figure from the theory, and is compared with the location obtained from schlieren and shadow photography in the experiments. These values agree over the entire range of subcritical Mach numbers, but not for the choked flow value, $M_\infty = 0.910$. It should be noted here that the technique for determining separation from the experiments cannot be considered to be accurate to more than 5% in x/c.

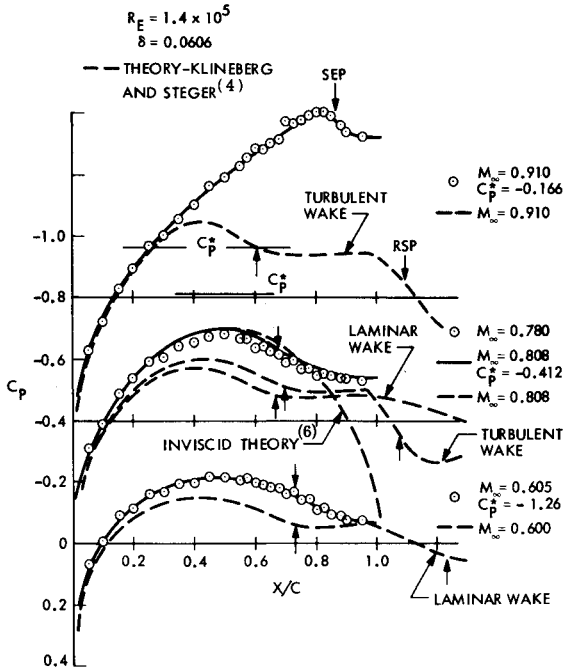

Fig. 4 Comparison of the pressure distribution on the 6% biconvex airfoil with the computations of Klineberg and Steger[4] for $Re = 1.4 \times 10^5$.

Figure 5 shows a comparison with the results of the computations by Klineberg and Steger[4] for $Re = 4.0 \times 10^4$. As in the previous case, the effects of viscosity are overpredicted near the midchord of the model. The flow for $M_\infty = 0.868$ exhibits a more extensive sonic zone than indicated by the theory; however, the plateau pressure is in somewhat better agreement than the supercritical results for $Re = 1.4 \times 10^5$.

It should be observed that the calculations indicate that the minimum value of C_p decreases with increasing Reynolds number, whereas the experiments for $M_\infty = 0.808$ indicate the opposite trend. The trend for the motion of the separation point upstream with increasing Reynolds number is accurately predicted, however. Despite the obvious disagreement between theory and experiment for the viscous flows presented here, these calculations represent the only successful attempt at computing viscous-inviscid interactions at transonic speeds, and properly predict the qualitative features of the flows involved despite disagreements in detail.

Conclusions

Results of the present experiments for Reynolds numbers $3.9 \times 10^4 \leqq Re \leqq 1.2 \times 10^6$ have been used to examine some of the effects of viscosity at transonic speeds. At low Reynolds numbers, the present results have been compared with the viscous-inviscid interaction theory of Klineberg and Steger,[4] and some differences are seen to exist between theory and experiment. In each case compared, the theoretical solution predicts a greater influence of viscosity, and consequently a lower value of the minimum pressure coefficient near the midchord of the body, than observed in experiment. The location of separation determined by optical measurements in the experiments agrees well with those predicted from theory, however.

References

[1] Ackeret, J., Feldmann, F., and Rott, N., "Investigations of Compression Shocks and Boundary Layers in Gases Moving at High Speed," TM 1113, Jan. 1947, NACA.

[2] Liepmann, H. W., Ashkenas, H., and Cole, J. D., "Experiments in Transonic Flow," Tech. Rept. 5667, Feb. 1948, Air Force Air Material Command, Wright-Patterson Air Force Base, Ohio.

[3] Alber, I. E., Bacon, J. W., Masson, B. S., and Collins, D. J., "An Experimental Investigation of Turbulent Transonic Viscous-Inviscid Interactions," *AIAA Journal*, Vol. 11, No. 5, May 1973, pp. 620–627.

[4] Klineberg, J. M. and Steger, J. L., "Calculation of Separated Flows at Subsonic and Transonic Speeds," *Lecture Notes in Physics*, Vol. 19, Springer-Verlag, New York, 1972, pp. 161–168.

[5] Collins, D. J., "An Inexpensive Technique for the Fabrication of Two-Dimensional Wind-Tunnel Models," *Review of Scientific Instruments*, Vol. 44, No. 7, July 1973, p. 855.

[6] Collins, D. J. and Krupp, J. A., "Experimental and Theoretical Investigations in Two-Dimensional Transonic Flow," *AIAA Journal*, Vol. 12, No. 6, June 1974, pp. 771–778.

[7] Collins, D. J. and Krupp, J. A., "Experimental and Theoretical Investigations in Two-Dimensional Transonic Flow," AIAA Paper 73-659, Palm Springs, Calif., 1973.

Stretch Time of Scribed Metal Diaphragms

S. K. CHAN*
Institute for Aerospace Studies, University of Toronto, Toronto, Canada

Introduction

DIAPHRAGMS are commonly used in shock tubes as quick-opening valves to release the high-pressure driver gas into the low-pressure channel. Ideally the diaphragm should open fully instantaneously. In practice the diaphragm opens in two stages; namely, the stretching stage and the petaling stage, each of which takes a finite time. In a conventional shock tube, the exact time the diaphragm starts to open is not critical to the operation. Therefore, the stretch time is immaterial. However, the petaling time has a strong influence on the shock-formation processes.[1,2] It is possible to estimate the petaling time of a scribed metal diaphragm from a number of analyses.[3-5] Nevertheless, there does not appear to be a theory dealing with diaphragm stretching. The stretch time of a diaphragm is a very important factor in the operation of devices such as the free-piston shock tube[6] and the UTIAS implosion-driven shock tube.[7,8] In particular, the UTIAS implosion driver is a dynamic system for which the timing of the implosion wave to match the diaphragm opening is very critical in order to obtain the maximum possible shock velocity, from a given driver condition. Otherwise, some of the implosion energy is dissipated in opening the diaphragm. Therefore, it is very important to have an estimate of the diaphragm stretch time. In the following analysis, only scribed metal diaphragms are considered. It can, however, be applied equally well to nonmetalic diaphragms.

Analysis

Figure 1a shows a sketch of a sectional view of a typical scribed diaphragm. The diaphragm is divided into two layers, 1 and 2,

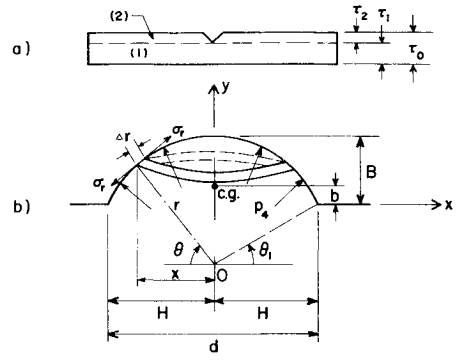

Fig. 1 Sketch of a section of the diaphragm and the stretching-diaphragm model.

with thickness τ_1 and τ_2, respectively. In the following analysis it is assumed that only Layer 1 exerts any resisting stress against stretching.

Consider an elemental ring with width Δr as shown in Fig. 1b. Pressure p_4 on the inside of the diaphragm exerts on the element a vertical force ΔF_p given by

$$\Delta F_p = 2\pi r^2 \cdot \cos\theta \cdot \sin\theta \, d\theta \cdot p_4 \tag{1}$$

The resultant vertical force ΔF_s due to circumferential stress σ_r on the two sides of the ring is given by

$$\Delta F_s = -2\pi\tau\sigma_r r \cdot \cos\theta \cdot \sin\theta \, d\theta \tag{2}$$

where τ is the instantaneous thickness of Layer 1 during the stretching process. The negative sign indicates a downward force. Apply Newton's second law to the vertical forces

$$\Delta F_p + \Delta F_s = \Delta m \, d^2y/dt^2 \tag{3}$$

where Δm is the mass of the elemental ring which includes the mass of Layer 2.

To obtain an estimate of stress σ_r we assume that the stretching diaphragm behaves as a section of a thin sphere with a uniform thickness. Equation (3) can then be integrated with r, τ, and σ_r a function of time t only

$$\int_{\theta_1}^{\pi/2} (\Delta F_p + \Delta F_s) = \int_{\theta_1}^{\pi/2} \Delta m \frac{d^2y}{dt^2} \tag{4}$$

where

$$\int_{\theta_1}^{\pi/2} \Delta F_p = \pi H^2 p_4 \tag{5}$$

and

$$\int_{\theta_1}^{\pi/2} \Delta F_s = -\pi \tau \sigma_r r \cos^2\theta_1 \tag{6}$$

with

$$\cos\theta_1 = 2BH/(H^2+B^2)$$
$$\tau = \tau_1 H^2/(H^2+B^2)$$

The right-hand side of Eq. (4) is simply

$$\int_{\theta_1}^{\pi/2} \Delta m \frac{d^2y}{dt^2} = \frac{d^2}{dt^2}\int_{\theta_1}^{\pi/2} \Delta m \cdot y = m\frac{d^2b}{dt^2} \tag{7}$$

where m is the total mass of the diaphragm and b is the distance of the c.g. of the bulging diaphragm from the base and $b = B/2$.

Substituting Eqs. (5–7) into Eq. (3) and letting $\eta = b/H$, after simplifying,

$$\frac{p_4}{\rho\tau_o H} - \frac{\tau_1}{\tau_o}\frac{\sigma_r}{\rho H^2}\frac{4\eta}{(1+4\eta^2)^2} = \frac{d^2\eta}{dt^2} \tag{8}$$

where ρ is the density of the diaphragm material. The stress-strain relationship in the plastic region can be represented by the usual form $\sigma_r = K\varepsilon_r^n$ where K is a stress proportionality constant and n is the strainhardening exponent. The tangential strain ε_r is related to the thickness strain ε_τ by the following

$$\varepsilon_1 + \varepsilon_2 + \varepsilon_\tau = 0 \tag{9}$$

Received December 19, 1973; revision received February 5, 1974. The work was financially supported by AFOSR (USA-AFOSR 72-2274B) and by NIC (Canada).

Index categories: Shock Waves and Detonations; Structural Dynamic Analysis.

* Graduate Student; presently Research Physicist at the Explosives Research Laboratory, Canadian Industries Limited, McMasterville, Quebec. Associate Member AIAA.